INTERNATIONAL JOURNAL FOR NUMERICAL METHODS IN FLUIDS
Int. J. Numer. Meth. Fluids 2005; **48**:115–133
Published online 17 December 2004 in Wiley InterScience (www.interscience.wiley.com). DOI: 10.1002/fld.816

Liquid vorticity computation in non-spherical bubble dynamics

A. A. Aganin[1,*,†] and N. A. Khismatullina[2]

[1]*Institute of Mechanics and Engineering, Kazan Science Center, Russian Academy of Science (IME KazSC RAS), Lobachevsky str., 2/31, Kazan 420111, Russia*
[2]*Kazan State Pedagogical University (KSPU), Mezhlauk str., 1, Kazan 420021, Russia*

SUMMARY

The purpose of this work is to compare efficiency of a number of numerical techniques of computation of liquid vorticity from non-spherical bubble oscillations. The techniques based on the finite-difference method (FDM), the collocation method (one with differentiating (CMd) the integral boundary condition and another without it (CM)) and the Galerkin method (GM) have been considered. The central-difference approximations are used in FDM. Sinus functions are chosen as the basis in GM. Problems of decaying a small distortion of the spherical shape of a bubble and dynamics of a bubble under harmonic liquid pressure variation with various parameters are used for comparison. The FDM technique has been found to be most efficient in all the cases. Copyright © 2004 John Wiley & Sons, Ltd.

KEY WORDS: bubble dynamics; viscosity; liquid vorticity; numerical methods

1. INTRODUCTION

Discovery of the periodic single bubble sonoluminescence in a standing acoustic wave [1, 2] and recently found phenomenon of nuclear emission during acoustic cavitation [3] stimulated investigation of dynamics of small gas bubbles in a liquid. The bubble shape, its deviation from the spherical one play an important role in bubble dynamics. With decreasing the bubble size the influence of the liquid viscosity on the bubble shape variation increases. Accurate approximation to description of the liquid viscosity effect within the full Navier–Stokes equations for the case of small deviation of the bubble shape from the sphere was proposed in Reference [4]. In that approximation, the deviation from the spherical shape is governed by a second-order ordinary differential equation which includes terms allowing for the liquid vorticity all over its area. The liquid vorticity is described by a one-dimensional partial differential

*Correspondence to: A. A. Aganin, Institute of Mechanics and Engineering, Kazan Science Center, Russian Academy of Science (IME KazSC RAS), Lobachevsky str., 2/31, Kazan 420111, Russia.
†E-mail: aganin@kfti.knc.ru

Contract/grant sponsor: Russian Foundation of Basic Research; contract/grant number: project 02-01-00100
Contract/grant sponsor: RAS

Received 24 January 2004
Revised 13 September 2004
Accepted 14 October 2004

equation (to some extent similar to that of heat conduction) with an integral boundary condition. Until recently the approximation of Prosperetti [4] has nearly not been used. Instead, some other mathematically simpler ways [5–11] of taking liquid vorticity into account have been utilized. All those ways are readily derived from Reference [4] by introducing some additional assumptions. Three main assumptions can be outlined. The first one assumes the liquid viscosity to be small so that the liquid vorticity on the bubble surface is only taken into account. The second one assumes the liquid viscosity to be large. This allows one to utilize the quasi-static distribution of the liquid vorticity. In the third assumption, the liquid vorticity is considered to be zero everywhere including the surface of the bubble. Also, some combinations of these assumptions are used. A concept of a thin viscous boundary layer is introduced to match different assumptions [10, 11]. The matching is performed through the value of the boundary layer thickness.

As a result, the description of the spherical shape distortion in References [5–11] is only comprised of an ordinary differential equation, which makes the analysis of a problem essentially simpler. At the same time, it has been shown in Reference [12] that additional simplifying assumptions may lead to significant errors in predicting the late stages of the bubble surface distortion decay.

In the general case of using the approximation of Prosperetti [4], numerical methods are necessary to find the solution to both the equation describing the distortion of the spherical shape of the bubble and that describing the liquid vorticity. From the computational point of view, the numerical procedure of solving the liquid vorticity equation is much more expensive. Therefore, the efficiency of such a numerical procedure is very important. By now several numerical techniques [12–16] have been used to solve the liquid vorticity equation. Unfortunately, there is no indication how those techniques differ in such an important criterion as their efficiency. In particular, the techniques based on the finite-difference method (FDM) are applied in References [12–15]. Many numerical aspects including those related to the efficiency of the numerical technique are not considered in References [12–14]. In Reference [15], these issues are discussed comprehensively enough but only for the technique suggested by the authors of Reference [15] without any comparison with others. A technique based on the collocation method (CM) is used in Reference [16]. The CM was chosen in Reference [16] according to earlier detailed investigation [17] of the efficiency of a number of numerical techniques for computing heat conduction inside the bubble and in the liquid around it. In particular, comparison of the efficiency of utilizing the FDM [14], Galerkin method (GM) and CM is presented in Reference [17]. Among those the adaptive Galerkin–Chebyshev spectral method was found to be the best, the FDM being the worst. Results of investigation of efficiency of heat conduction computation cannot be directly applied to the case with vorticity because their mathematical descriptions are to a large extent different. In particular, unlike the case with the temperature, the boundary condition in the case of the liquid vorticity is of integral character. Therefore, a special study is necessary to estimate efficiency of different ways of the liquid vorticity computation.

The purpose of this work is to compare the efficiency of a number of numerical techniques of the liquid vorticity computation within the approximation of Prosperetti [4]. The techniques based on the FDM [15], the CM (including its variant similar to that used in Reference [16]) and the GM are considered. In the technique of Aganin *et al.* [15], central finite-differences are used to approximate the derivatives. In the technique based on the GM sinus-functions are taken as the basis. The efficiency of the techniques is estimated by comparing their results of

computing two problems: decay of a small distortion of the spherical surface of a bubble and dynamics of a bubble under harmonic liquid pressure variation. Various values of the liquid viscosity and the pressure variation amplitude are considered. In all the cases, the technique based on the FDM has been found to be most preferable.

2. NUMERICAL TECHNIQUES

2.1. Problem statement

Dynamics of a gas bubble in a viscous liquid is considered within the problem statement of Prosperetti [4]. In that statement, the bubble surface equation is

$$r = R(t) + \sum_{i=2}^{\infty} a_i(t) Y_i(\theta, \varphi) \tag{1}$$

where r, θ, φ are the spherical co-ordinates with the origin in the bubble centre, t the time, Y_i the spherical surface harmonic of number i, $a_i(t)$ the amplitude of the corresponding deviation from the spherical shape $r = R$, R the mean value of the radial co-ordinates of the bubble surface, being called below the bubble radius. Distortion of the spherical bubble shape is assumed small $|a_i(t)|/R(t) \ll 1$, $i = 2, 3, \ldots$.

The bubble radius $R(t)$ and the deviation amplitude $a_i(t)$ are governed by the following equations:

$$\left(1 - \frac{\dot{R}}{c_0} + \frac{4\nu}{c_0 R}\right) R\ddot{R} + \frac{3}{2}\left(1 - \frac{\dot{R}}{3c_0}\right)\dot{R}^2 = \left(1 + \frac{\dot{R}}{c_0}\right)\frac{p_b - p_\infty}{\rho_0} - \frac{4\nu\dot{R}}{R} - \frac{2\sigma}{\rho_0 R} \tag{2}$$

$$R\ddot{a}_i + \left[3\dot{R} + 2(i+1)(i+2)\frac{\nu}{R}\right]\dot{a}_i - (i-1)\left[\ddot{R} - 2(i+2)\frac{\dot{R}\nu}{R^2} - \frac{\sigma}{\rho_0 R^2}(i+1)(i+2)\right] a_i + 2\nu i(i+2)(2i+1)R^{i-2}\alpha_i + i(i+1)\frac{\dot{R}}{R}\beta_i = 0 \tag{3}$$

where ρ_0, c_0 are the density and the sound speed in the liquid, respectively, ν the kinematic liquid viscosity, σ the surface tension, p_b the gas pressure in the bubble, p_∞ the liquid pressure at large distance from the bubble,

$$\alpha_i = -\frac{i+1}{2i+1}\int_R^\infty T_i(r,t) r^{-i}\,\mathrm{d}r, \quad \beta_i = \int_R^\infty \left[\left(\frac{R}{r}\right)^3 - 1\right]\left(\frac{R}{r}\right)^i T_i(r,t)\,\mathrm{d}r$$

The function $T_i(r,t)$ is determined by the expression

$$\nabla \times \left(\sum_{i=2}^{\infty} T_i(r,t) Y_i(\theta,\varphi) \right) \mathbf{e}_1 = \nabla \times \mathbf{u}$$

where $\mathbf{e}_1$ is the unit vector of the radial co-ordinate, $\mathbf{u}$ the vector of the liquid velocity.

The function $T_i(r,t)$ characterizes the toroidal component of the liquid vorticity. In the general case the liquid vorticity $\mathbf{\Omega}$ can be presented as $\mathbf{\Omega} = \mathbf{S} + \mathbf{T}$ [4], where $\mathbf{S}$ is the poloidal component. If $\mathbf{S} = 0$ at $t = 0$ then $\mathbf{S} = 0$ at $t > 0$ [4]. The assumption $\mathbf{S} = 0$ at $t = 0$ is used in this paper.

The gas pressure in the bubble p_b and the liquid pressure p_∞ vary as follows:

$$p_b = p_b^0 \left(\frac{R_0^3 - AR_0^3}{R^3 - AR_0^3} \right)^\gamma, \quad p_b^0 = p_0 + \frac{2\sigma}{R_0} \tag{4}$$

$$p_\infty = p_0 - \Delta p \sin \omega t \tag{5}$$

In (4), (5), A is a constant, R_0 the initial radius of the bubble, p_0 the static pressure in the liquid, Δp and ω are the amplitude and the frequency of oscillation of the pressure p_∞, respectively.

The function $T_i(r,t)$ is governed by the equation

$$\frac{\partial T_i}{\partial t} + \dot{R} R^2 \frac{\partial}{\partial r} \left(\frac{T_i}{r^2} \right) + \nu \left(\frac{i(i+1)T_i}{r^2} - \frac{\partial^2 T_i}{\partial r^2} \right) = 0 \tag{6}$$

subject to the boundary conditions

$$T_i(R,t) = \frac{2}{i+1} \left[(i+2)\dot{a}_i - (i-1)\frac{\dot{R}}{R} a_i + (2i+1)R^{i-1}\alpha_i \right] \tag{7a}$$

$$T_i(\infty,t) = 0 \tag{7b}$$

The initial conditions for Equations (2)–(7) are

$$R(0) = R_0, \quad \dot{R}(0) = 0, \quad a_i(0) = a_i^0, \quad \dot{a}_i(0) = 0, \quad T(r,0) = 0 \tag{8}$$

All the numerical techniques studied below use the following change of variables:

$$\xi = R/r, \quad \tau = t$$

In new variables, Equations (6), (7) take the form

$$\frac{\partial T_i}{\partial \tau} + \left[\frac{\dot{R}}{R}(\xi - \xi^4) - \frac{2\nu}{R^2}\xi^3 \right] \frac{\partial T_i}{\partial \xi} - \frac{\nu \xi^4}{R^2} \frac{\partial^2 T_i}{\partial \xi^2} + \xi^2 \left[\frac{\nu i(i+1)}{R^2} - \frac{2\dot{R}}{R}\xi \right] T_i = 0 \tag{9}$$

$$T_i(0,\tau) = 0 \tag{10a}$$

$$T_i(1,\tau) = \frac{2}{i+1} \left[(i+2)\dot{a}_i - (i-1)\frac{\dot{R}}{R} a_i - (2i+1)R^{i-1}\alpha_i \right] \tag{10b}$$

where

$$\alpha = -\frac{(i+1)R^{1-i}}{2i+1}\int_0^1 \xi^{i-2}T_i\,\mathrm{d}\xi, \quad \beta = R\int_0^1 (\xi^3-1)\xi^{i-2}T_i\,\mathrm{d}\xi$$

While presenting numerical techniques of solving (9), (10) the lower index i indicating the number of the spherical harmonic is omitted, i.e. $T(\xi,\tau)$ stands for $T_i(\xi,\tau)$, etc.

2.2. A technique based on the FDM

In this technique, the interval $0 \leqslant \xi \leqslant 1$ is divided into N equal subintervals by the points $\xi_0 = 0$, $\xi_{k+1} = \xi_k + \Delta\xi$, $k = 1,\ldots,N$ where $\Delta\xi = 1/N$. The following approximations are taken for the spatial derivatives and the integrals:

$$(T_\xi)_k = \frac{T_{k+1}-T_{k-1}}{2\Delta\xi}, \quad (T_{\xi\xi})_k = \frac{T_{k+1}-2T_k+T_{k-1}}{\Delta\xi^2}$$

$$\int_0^1 \xi^{i-2}T\,\mathrm{d}\xi = \sum_{k=1}^{N}(\xi_k^{i-2}T_k + \xi_{k+1}^{i-2}T_{k+1})\frac{\Delta\xi}{2}$$

$$\int_0^1 (\xi^3-1)\xi^{i-2}T\,\mathrm{d}\xi = \sum_{k=1}^{N}[(\xi_k^3-1)\xi_k^{i-2}T_k + (\xi_{k+1}^3-1)\xi_{k+1}^{i-2}T_{k+1}]\frac{\Delta\xi}{2}$$

where the lower index k indicates the value of the corresponding function at ξ_k. Equation (9) leads to the $N-1$ ordinary differential equations

$$\dot{T}_k + \frac{A_k}{2\Delta\xi}(T_{k+1}-T_{k-1}) - \frac{B_k}{\Delta\xi^2}(T_{k+1}-2T_k+T_{k-1}) + C_kT_k = 0 \tag{11}$$

where $k = 2,\ldots,N$,

$$\alpha = -\frac{(i+1)R^{1-i}}{2i+1}\,\frac{\Delta\xi}{2}\sum_{k=1}^{N}(\xi_k^{i-2}T_k + \xi_{k+1}^{i-2}T_{k+1})$$

$$\beta = R\,\frac{\Delta\xi}{2}\sum_{k=1}^{N}[(\xi_k^3-1)\xi_k^{i-2}T_k + (\xi_{k+1}^3-1)\xi_{k+1}^{i-2}T_{k+1}]$$

$$T_1 = 0$$

$$T_{N+1} = \frac{2}{i+1}\left\{(i+2)\dot{a} - (i-1)\frac{\dot{R}}{R}a - \frac{(i+1)\Delta\xi}{2}\sum_{k=1}^{N}(\xi_k^{i-2}T_k + \xi_{k+1}^{i-2}T_{k+1})\right\}$$

$$A_k = \frac{\dot{R}}{R}(\xi_k - \xi_k^4) - \frac{2\nu}{R^2}\xi_k^3, \quad B_k = \frac{\nu}{R^2}\xi_k^4, \quad C_k = \xi_k^2\left[\frac{\nu}{R^2}i(i+1) - 2\frac{\dot{R}}{R}\xi_k\right]$$

In the technique based on the FDM, the solution to problem (2), (3), (6)–(8) is found numerically by solving Equations (2), (3), (11) by the Dorman–Prince method [18] under initial conditions (8).

2.3. A technique based on the GM

While using the GM, the homogeneous boundary conditions are known to be more preferable. This is derived here by introducing the function $Q(\xi,\tau)=T(\xi,\tau)-\xi T(1,\tau)$. Then

$$Q(0,\tau)=Q(1,\tau)=0$$

and

$$T(\xi,\tau)=Q(\xi,\tau)+\xi T(1,\tau) \tag{12}$$

It is easy to see that

$$T(1,\tau)=\frac{i}{i+2}\left(A-2\int_0^1 \xi^{i-2}Q\,\mathrm{d}\xi\right) \tag{13}$$

and that

$$\alpha=-\frac{i+1}{(i+2)(2i+1)R^{i-1}}\left(A+i\int_0^1 \xi^{i-2}Q\,\mathrm{d}\xi\right)$$

$$\beta=R\int_0^1 \xi^{i+1}Q\,\mathrm{d}\xi-\frac{Ri(i+5)}{(i+2)(i+3)}\int_0^1 \xi^{i-2}Q\,\mathrm{d}\xi-\frac{3RA}{(i+2)(i+3)}$$

where

$$A=\frac{2}{i+2}\left[(i+2)\dot{a}-(i-1)\frac{\dot{R}}{R}a\right]$$

Substitution of (12) into (9) gives

$$\begin{aligned}
&Q_\tau-\frac{2i}{i+2}\,\xi\int_0^1 \xi^{i-2}Q_\tau\,\mathrm{d}\xi+\left[\frac{\dot{R}}{R}(\xi-\xi^4)-\frac{2v}{R^2}\,\xi^3\right]Q_\xi-\frac{v}{R^2}\,\xi^4Q_{\xi\xi}\\
&+\xi^2\left[\frac{v}{R^2}\,i(i+1)-2\,\frac{\dot{R}}{R}\,\xi^3\right]Q+\frac{i\dot{A}}{i+2}\,\xi\\
&+\frac{i}{i+2}\left\{\left[\frac{\dot{R}}{R}(\xi-\xi^4)-\frac{2v}{R^2}\,\xi^3\right]+\xi^3\left[\frac{v}{R^2}\,i(i+1)-2\,\frac{\dot{R}}{R}\,\xi^3\right]\right\}\\
&\times\left(A-2\int_0^1 \xi^{i-2}Q\,\mathrm{d}\xi\right)=0
\end{aligned} \tag{14}$$

According to the GM, the unknown function $Q(\xi,\tau)$ is presented in the form

$$Q(\xi,\tau)\approx\sum_{k=1}^{N} b_k(\tau)H_k(\xi) \tag{15}$$

where $b_k(\tau)$ are unknown coefficients, $H_k(\xi)$ the basis functions satisfying the homogeneous boundary conditions $H_k(0)=H_k(1)=0$. Substitution of (15) into (14) leads to

$$\delta=\sum_{k=1}^{N}u_k\dot{b}_k+\sum_{k=1}^{N}v_kb_k+w$$

where

$$u_k=H_k-\frac{2i\xi}{i+2}\int_0^1\xi^{i-2}H_k\,\mathrm{d}\xi$$

$$v_k=\left[\frac{\dot{R}(\xi-\xi^4)}{R}-\frac{2\nu\xi^3}{R^2}\right]H_k'-\frac{\nu\xi^4}{R^2}H_k''+\xi^2\left[\frac{\nu i(i+1)}{R^2}-\frac{2\dot{R}\xi}{R}\right]H_k$$
$$-\frac{i}{i+2}\left[\frac{\dot{R}(\xi-\xi^4)}{R}-\frac{2\nu\xi^3}{R^2}+\xi^3\left(\frac{\nu i(i+1)}{R^2}-\frac{2\dot{R}\xi}{R}\right)\right]\left(\int_0^1\xi^{i-2}H_k\,\mathrm{d}\xi\right)$$

$$w=\frac{i\dot{A}\xi}{i+2}+\frac{iA}{i+2}\left\{\left[\frac{\dot{R}(\xi-\xi^4)}{R}-\frac{2\nu\xi^3}{R^2}\right]+\xi^3\left[\frac{\nu i(i+1)}{R^2}-2\frac{\dot{R}\xi}{R}\right]\right\}$$

Differential equations in $b_k(\tau)$, $k=1,2,\ldots,N$ are determined by the scalar products $(\delta,H_m)=0$, $m=1,2,\ldots,N$, where $(a,b)=\int_0^1 ab\,\mathrm{d}\xi$. In the matrix form these equations can be written as

$$\mathbf{P}\dot{\mathbf{b}}+\mathbf{A}\mathbf{b}+\mathbf{c}=0 \tag{16}$$

where $\mathbf{b}$, $\dot{\mathbf{b}}$, $\mathbf{c}$, $\mathbf{P}$, $\mathbf{A}$ are vectors and matrices with the elements b_m, $\dot{b}_m$, $c_m=(w,H_m)$, $p_{m,k}=(u_k,H_m)$, $a_{m,k}=(v_k,H_m)$, respectively. We take $H_k(\xi)=\sin k\pi\xi$, which gives the diagonally predominant matrix $\mathbf{P}$.

In the technique based on the GM, the solution to problem (2), (3), (6)–(8) is found numerically by solving Equations (2), (3), (16) by the Dorman–Prince method [18] under initial conditions (8).

2.4. Two techniques based on the CM

In these techniques, the unknown function $T(\xi,\tau)$ is presented in the form [16]

$$T(\xi,\tau)\approx\sum_{k=0}^{N}u_k(\tau)H_{2k}(\xi) \tag{17}$$

where $H_{2k}(\xi)$ are the Chebyshev polynomials of even order. Then

$$\alpha=-\frac{i+1}{(2i+1)R^{i-1}}\sum_{k=0}^{N}u_k\int_0^1\xi^{i-2}H_{2k}(\xi)\,\mathrm{d}\xi$$
$$\beta=R\sum_{k=0}^{N}u_k\left(\int_0^1\xi^{i+1}H_{2k}(\xi)\,\mathrm{d}\xi-\int_0^1\xi^{i-2}H_{2k}(\xi)\,\mathrm{d}\xi\right) \tag{18}$$

The collocation points are chosen as $\xi_m=\cos\pi m/2N$, $m=1,2,\ldots,N$.

One can see that the boundary point $\xi = 0$ is included in the set of the collocation points with $m = N$. This is a convenient way of satisfying boundary condition (10a). It is based on the fact that at $\xi = 0$, Equation (9) is reduced to expression $\partial T(0,\tau)/\partial\tau = 0$ resulting from differentiating boundary condition (10a).

By substituting (17) into (9) and putting $\xi = \xi_m$, $m = 1, 2, \ldots, N$, one can obtain N ordinary differential equations

$$\sum_{k=0}^{N} \dot{u}_k H_{2k}(\xi_m) + \sum_{k=0}^{N} u_k \left[\left(\frac{\dot{R}}{R}(\xi_m - \xi_m^4) - \frac{2v}{R^2}\,\xi_m^3 \right) H'_{2k}(\xi_m) \right.$$

$$\left. - \frac{v}{R^2}\,\xi_m^4 H''_{2k}(\xi_m) + \xi_m^2 \left(\frac{v}{R^2}\,i(i+1) - 2\,\frac{\dot{R}}{R}\,\xi_m \right) H_{2k}(\xi_m) \right] = 0 \tag{19}$$

in $N + 1$ unknowns $u_0, u_1, \ldots, u_N$. One more equation is necessary to close the set of Equations (19). Therefore, boundary condition (10b) is used for closing. Two methods of closing are considered, one being exactly the same as that in Reference [16].

Method 1. One of the unknowns $u_0, u_1, \ldots, u_N$, namely u_0, is expressed in terms of the others directly from (7a). Taking into account that $H_m(1) = 1$ for any m one can write

$$u_0 = \frac{i-1}{i+1} \left(A - \sum_{k=1}^{N} u_k (1 + 2I_{i,k}) \right) \tag{20}$$

where

$$I_{i,k} = \int_0^1 \xi^{i-2} H_{2k}(\xi)\,\mathrm{d}\xi, \quad A = \frac{2}{i+2} \left[(i+2)\dot{a} - (i-1)\frac{\dot{R}}{R}\,a \right]$$

Substitution of (20) into (19) leads to N ordinary differential equations in N unknowns u_k

$$\sum_{k=1}^{N} \dot{u}_k \left[H_{2k}(\xi_m) - \frac{i-1}{i+1}(1 + 2I_{i,k}) \right]$$

$$+ \sum_{k=1}^{N} u_k \left\{ \left(\frac{\dot{R}}{R}(\xi_m - \xi_m^4) - \frac{2v}{R^2}\,\xi_m^3 \right) H'_{2k}(\xi_m) - \frac{v}{R^2}\,\xi_m^4 H''_{2k}(\xi_m) \right.$$

$$\left. + \xi_m^2 \left(\frac{v}{R^2}\,i(i+1) - 2\,\frac{\dot{R}}{R}\,\xi_m \right) \left[H_{2k}(\xi_m) - \frac{i-1}{i+1}(1 + 2I_{i,k}) \right] \right\}$$

$$- \frac{i-1}{i+1} \left[\dot{A} + A\xi_m^2 \left(\frac{v}{R^2}\,i(i+1) - 2\,\frac{\dot{R}}{R}\,\xi_m \right) \right] = 0 \tag{21}$$

Method 2 [16]. Boundary condition (10b) is differentiated with respect to τ to obtain

$$\dot{T}(1,\tau) = \frac{2}{i+1} \left[(i+2)\ddot{a} - (i-1) \left(\frac{\ddot{R}}{R}\,a - \frac{\dot{R}^2}{R^2}\,a + \frac{\dot{R}}{R}\,\dot{a} \right) - (i+1) \int_0^1 \xi^{i-2} T_\tau\,\mathrm{d}\xi \right] \tag{22}$$

The set of equations (19) is closed by the equation

$$\sum_{k=0}^{N} \dot{u}_k - \sum_{k=0}^{N} u_k \left[(i-1)\frac{\dot{R}}{R} + \frac{2iv}{R^2} - \frac{8vk^2}{R^2} + \frac{2i\dot{R}}{R} \int_0^1 \xi^{i+1} H_{2k}(\xi)\, \mathrm{d}\xi \right]$$

$$-\frac{2(i+2)}{i+1}\ddot{a} + \frac{2(i-1)}{i+1}\frac{\ddot{R}}{R}a + \frac{2(i-1)(i+3)}{i+1}\frac{\dot{R}}{R}\dot{a} - \frac{2i(i-1)}{i+1}\frac{\dot{R}^2}{R^2}a = 0 \qquad (23)$$

which is derived from (22) by using (20), (9), (18) and taking into account that $H_k(1)=1$ and $H_k'(1)=k^2$. The integrals in (18), (21) and (23) can be evaluated exactly.

Thus, two techniques based on the CM are considered, with (CMd) and without (CM) differentiation of the integral boundary condition. The solution to problem (2), (3), (6)–(8) is found numerically by solving Equations (2), (3), (19), (23) in the first one and Equations (2), (3), (21) in the second one. In both cases the numerical solution is obtained by the Dorman–Prince method [18] under initial conditions (8).

3. RESULTS

This section presents results of investigation of four numerical techniques for solving problem (2)–(8). In particular, the FDM, GM, CMd, and CM techniques based on the finite difference (FDM), Galerkin (GM) methods and the CM with (CMd) and without (CM) differentiation of the integral boundary condition are considered. They have been described in Sections 2.1– 2.3. Convergence of numerical solution with increasing the number of grid cells in the FDM technique, the number of the basis functions in the GM technique and the number of the collocation points in the CMd and CM techniques is investigated in view of comparison of their efficiency with respect to the computational time consumption. The efficiency is compared using two typical bubble dynamics problems: decay of a small distortion of the spherical bubble shape and dynamics of a bubble with a small deviation from the spherical shape under harmonic liquid pressure variation. The following criterion

$$\max_{0 \leqslant t \leqslant t_f} |\lg |a_{i,N_2}/a_i^0| - \lg |a_{i,N_1}/a_i^0|| < \varepsilon \qquad (24)$$

is taken for numerical convergence. In (24), $a_{i,N} = a_{i,N}(t)$ is the value of $a_i(t)$ computed with N grid points in the FDM technique, N the basis functions in the GM technique, and N the collocation points in the CMd and CM techniques, N_1, N_2 are values of N, ε is a small positive number, t_f the time instant.

3.1. Problem 1: decay of a small distortion of the spherical bubble shape

At $t<0$ a gas bubble with a small distortion of the spherical shape in the form of the ith harmonic Y_i ($a_i \neq 0$) rests in a viscous liquid. The distortion of the bubble shape is supplied by the action of some surface forces equilibrating the action of the surface tension. At the instant $t=0$ the action of the equilibrating forces suddenly terminates. As a result, the bubble shape starts oscillating. With time the amplitude of these oscillations decreases due

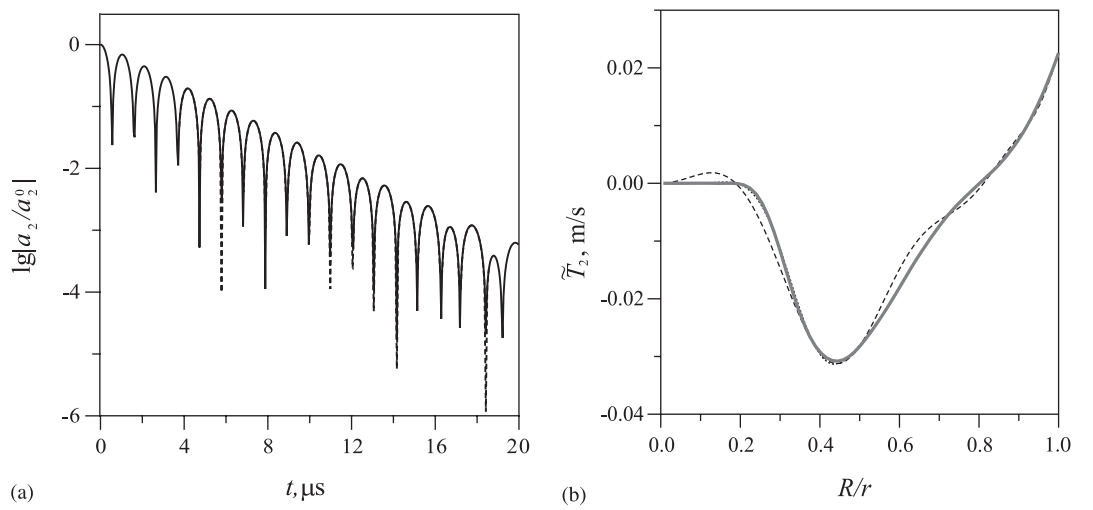

Figure 1. Time-dependences of the relative bubble shape distortion amplitude logarithm $\lg|a_2/a_2^0|$ in $0 \leqslant t \leqslant t_f$. (a) $N = 8$—dotted curve, 16—solid curve) and spatial distributions of the liquid vorticity function $\tilde{T}_2(\xi, \tau)$ at the instant t_f, (b) $N = 8$—dashed curve, 16—dotted curve, 24—solid curve) by the CM technique under $\nu = 0.5 \times 10^{-6}$ m^2/s, $t_f = 20$ μs.

to the liquid viscosity. The liquid pressure p_∞ far from the bubble and the bubble radius R remain constant. The problem is considered under the following data: $i = 2$, $\sigma = 0.073$ N/m, $\rho_0 = 10^3$ kg/m^3, $c_0 = 1500$ m/s, $a_2^0 = 10^{-3} R_0$, $\dot{R}(0) = 0$, $\dot{a}_2(0) = 0$, $T_2(r, 0) = 0$, $R_0 = 4.5$ μm, $\nu/\nu_* = 0.5$, $\nu_* = 10^{-6}$ m^2/s (ν_* is an auxiliary parameter), $p_0 = 1$ bar, $\omega = 0$, $\Delta p = 0$.

Figures 1 and 2 illustrate some features of the numerical convergence of the CM technique with increasing the number N and the temporal interval $0 \leqslant t \leqslant t_f$. Time-dependences of the relative distortion amplitude logarithm $\lg|a_2/a_2^0|$ and the spatial distributions of the function $\tilde{T}_2 = T_2(\xi, \tau) R_0/a_2^0$ characterizing the liquid vorticity at the instant t_f are given in Figures 1(a), 2(a) and Figures 1(b), 2(b), respectively. Figure 1 illustrates the numerical convergence in the interval $0 \leqslant t \leqslant t_f = 20$ μs while Figure 2 in $0 \leqslant t \leqslant t_f = 100$ μs.

In Figures 1 and 2, graphical coincidence of curves of different N is observed for the time-dependences of $\lg|a_2/a_2^0|$ in $0 \leqslant t \leqslant t_f$ under somewhat smaller values of N than it is for the spatial distributions of $\tilde{T}_2(\xi, \tau)$. This is due to the fact that, according to (3), the influence of the liquid vorticity on the bubble shape distortion is of integral character. One can also notice in Figures 1 and 2 that the more the length of the temporal interval $0 \leqslant t \leqslant t_f$ the greater the value of N required for computing numerical solution of the prescribed accuracy. Similar properties but with some slight differences are also manifested by other numerical techniques under consideration (FDM, GM, CMd). More detailed information (but in the less pictorial form) about efficiency of each technique is given in Tables I and II.

Table I contains the computational time consumption T, i.e. the time required for numerical solution of problem 1 up to the instant t_f, the instant t_f and a few values of N. The computational time consumption T is presented in dimensionless units relative to the amount of

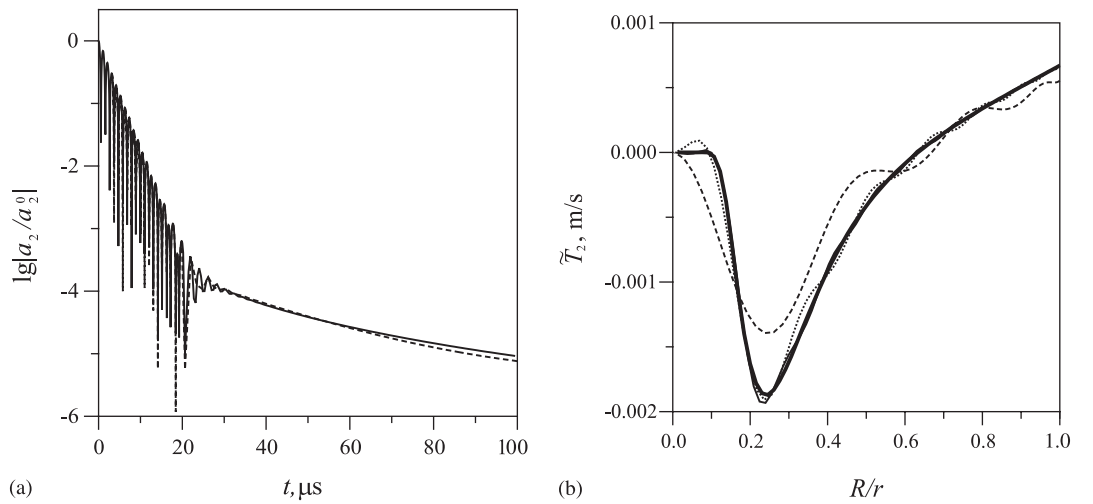

Figure 2. Same as in Figure 1 but under $t_f = 100\,\mu s$ and in (b) thin solid curve corresponds to $N = 24$, solid curve to $N = 48$.

Table I. Computational time consumption T of a technique to solve problem 1 in $0 \leqslant t \leqslant t_f$ under some N and t_f.

		Technique			
t_f (μs)	N	FDM	GM	CMd	CM
20	8	<1	10	2	5
	16	<1	12	30	75
	24	<1	15	230	450
	32	<1	35	1000	1700
	48	1	130	9500	13 100
100	8	<1	22	7	8
	16	1	37	150	150
	24	1	77	1080	1100
	32	2	180	5000	5300
	48	4		$>4.7 \times 10^4$	46 982

Table II. N and T required by a technique to solve problem 1 in $0 \leqslant t \leqslant t_f$ with criterion (24) where $\varepsilon = 10^{-3}$ under some t_f.

	Technique							
	FDM		GM		CMd		CM	
t_f (μs)	N	T	N	T	N	T	N	T
20	16	<1	16	15	16	30	16	73
100	16	1	24	80	>48	$>4.7 \times 10^4$	32	1100

computational time necessary for numerical solution of problem 1 up to the instant $t_f = 100\,\mu s$ by the FDM technique under $N = 16$. One can see in Table I that under a fixed value of N the FDM technique requires the least computational time. In the descending order in T, the FDM technique is followed (in most cases) by the GM one, then the CMd and CM ones come.

The values of N and T for numerical solution of problem 1 with criterion (24) where $\varepsilon = 10^{-3}$ are shown in Table II. It can be seen that the numerical convergence of all the techniques except the CMd one is nearly equal. Their numerical solutions satisfy criterion (24) with the prescribed accuracy under $N = 16$ or 24. Table II allows one to conclude that the most efficient technique is that based on the FDM, and then the GM one comes. The technique based on the CM with integral boundary condition differentiation [16] works better than that without differentiation only when $t_f = 20\,\mu s$. When $t_f = 100\,\mu s$ the time consumption of the CMd technique becomes really enormous.

Thus, the results presented above allow one to conclude that while solving the problem of decaying a small distortion of the spherical shape of the bubble surface the FDM technique in every respect appears to be significantly more efficient.

3.2. Problem 2: dynamics of a bubble under harmonic liquid pressure variation

The only difference between the statements of this problem and problem 1 is that at $t = 0$ the liquid pressure p_∞ far from the bubble begins here varying according to harmonic law (4). Variation of p_∞ leads to oscillations of the bubble radius R. Variation of R influences the temporal behaviour of the deviation amplitude a_i. With increasing the pressure oscillation amplitude Δp this influence increases.

Problem 2 is considered for the data typical of the SBSL regime [1, 2]: $i = 2$, $\sigma = 0.073\,\mathrm{N/m}$, $\nu = 10^{-6}\,\mathrm{m^2/s}$, $\rho_0 = 10^3\,\mathrm{kg/m^3}$, $c_0 = 1500\,\mathrm{m/s}$, $a_2^0 = 10^{-3} R_0$, $\dot{R}(0) = 0$, $\dot{a}_2(0) = 0$, $T_2(r, 0) = 0$, $\omega/2\pi = 26\,400\,\mathrm{Hz}$, $R_0 = 7\,\mu m$, $p_0 = 1\,\mathrm{bar}$. The oscillation amplitude Δp of the liquid pressure p_∞ far from the bubble is taken to be 0.5, 1 and 3 bar.

Figures 3–8 illustrate features of numerical convergence of the FDM technique with increasing the number N and the time interval $0 \leqslant t \leqslant t_f$ under $\Delta p/p_0 = 0.5$, 1 and 3. Figures 3 and 4 correspond to $\Delta p/p_0 = 0.5$, Figures 5 and 6 to $\Delta p/p_0 = 1$, and Figures 7 and 8 to $\Delta p/p_0 = 3$. Figures 3(a)–8(a) present time-dependences of the relative distortion amplitude logarithm $\lg|a_2/a_2^0|$ and the bubble radius R in the interval $0 \leqslant t \leqslant t_f$. Figures 3(b)–8(b) show the spatial distributions of the liquid vorticity function $\tilde{T}_2 = T_2(\xi, \tau) R_0/a_2^0$ at the instant t_f. Figures 3, 5 and 7 are for $t_f = 40\,\mu s$, Figures 4, 6 and 8 for $t_f = 100\,\mu s$.

The bubble shape oscillations are stable under $\Delta p/p_0 = 0.5$, 1 and they are unstable under $\Delta p/p_0 = 3$. The value $\Delta p/p_0 = 1$ is the closest to the stability boundary. Under $\Delta p/p_0 = 0.5$ the influence of the external excitation on the time-dependences of $\lg|a_2/a_2^0|$ and the spatial distributions of $\tilde{T}_2(\xi, \tau)$ is insignificant: the corresponding curves in Figures 3 and 4 are qualitatively similar to those presented in Figures 1 and 2 for problem 1 without any external excitation.

As for problem 1, graphical coincidence of the curves of $\lg|a_2/a_2^0|$ is observed in Figures 3–8 at somewhat smaller values of N than it is for the curves of $\tilde{T}_2(\xi, \tau)$ and the difference in curves of the same N increases with increasing t_f. These features of the FDM technique are also typical of other techniques. More detailed information characterizing the efficiency of all the techniques is given in Tables III–V.

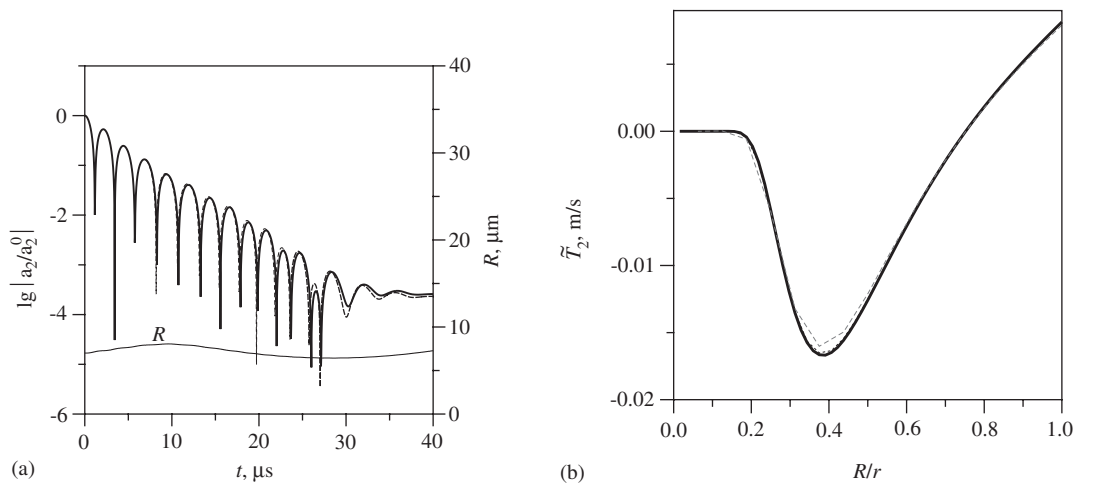

Figure 3. Time-dependences of the relative bubble shape distortion amplitude logarithm $\lg|a_2/a_2^0|$ and the bubble radius R in $0 \leqslant t \leqslant t_f$. (a) $N = 8$—dotted curve, 16—solid curve) and spatial distributions of the liquid vorticity function $\tilde{T}_2(\xi, \tau)$ at the instant t_f, (b) $N = 16$—dashed curve, 32—dotted curve, 64—solid curve) by the FDM technique under $\Delta p = 0.5$ bar, $t_f = 40$ μs.

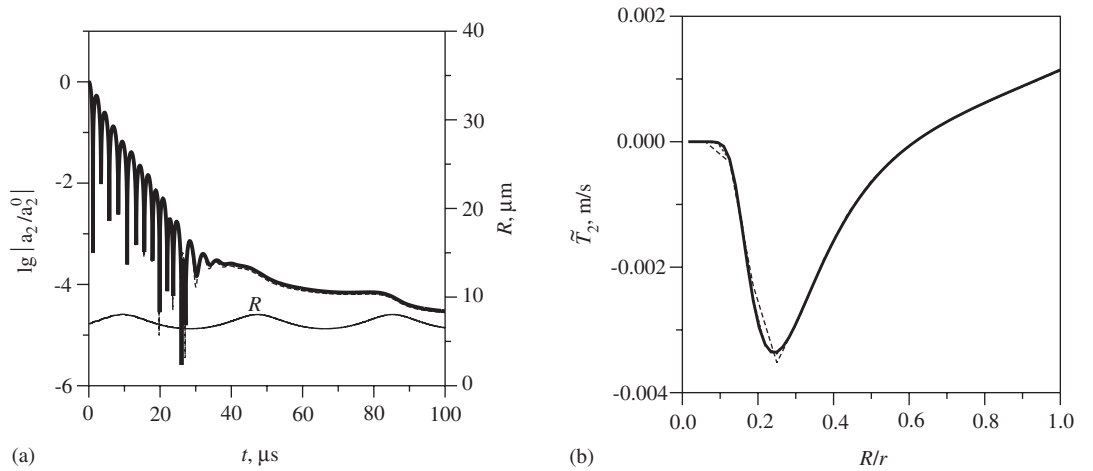

Figure 4. Same as in Figure 3 but under $t_f = 100$ μs and in (a) solid curve corresponds to $N = 32$.

Tables III and IV contain the computational time consumption T required to numerically solve problem 2 up to the instant t_f under a few values of N and three values of Δp for $t_f = 40$ and 100 μs, respectively. The data of these tables shows again that at a fixed N the FDM technique consumes the least amount of the computational time, then, in ascending order of T (in the most cases) the GM technique comes, followed by the CMd and CM ones.

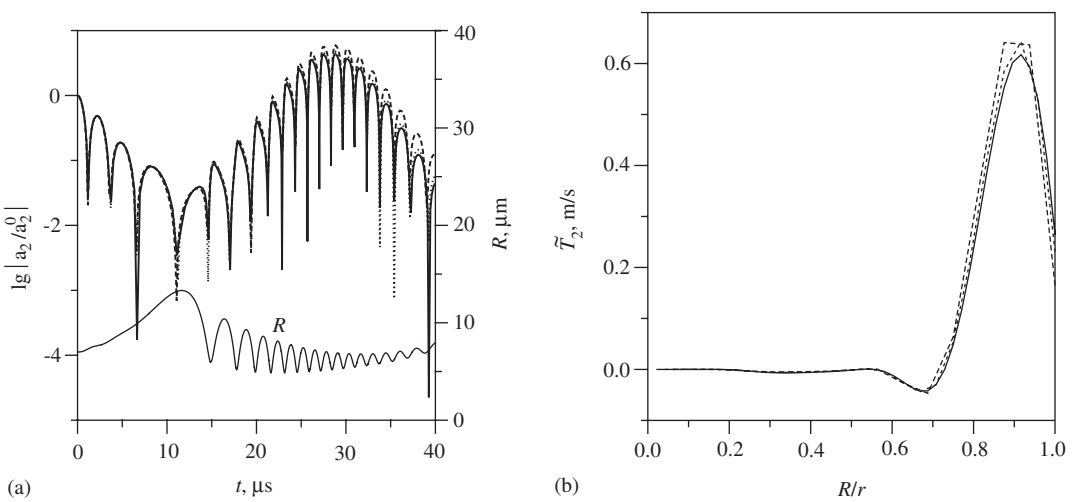

Figure 5. Time-dependences of the relative bubble shape distortion amplitude logarithm $\lg|a_2/a_2^0|$ and the bubble radius R in $0 \leqslant t \leqslant t_f$. (a) $N = 8$—dotted curve, 16—dashed curve, 32—solid curve) and spatial distributions of the liquid vorticity function $\tilde{T}_2(\xi, \tau)$ at the instant t_f, (b) $N = 16$—dashed curve, 32—dotted curve, 48—solid curve) by the FDM technique under $\Delta p = 1$ bar, $t_f = 40$ μs.

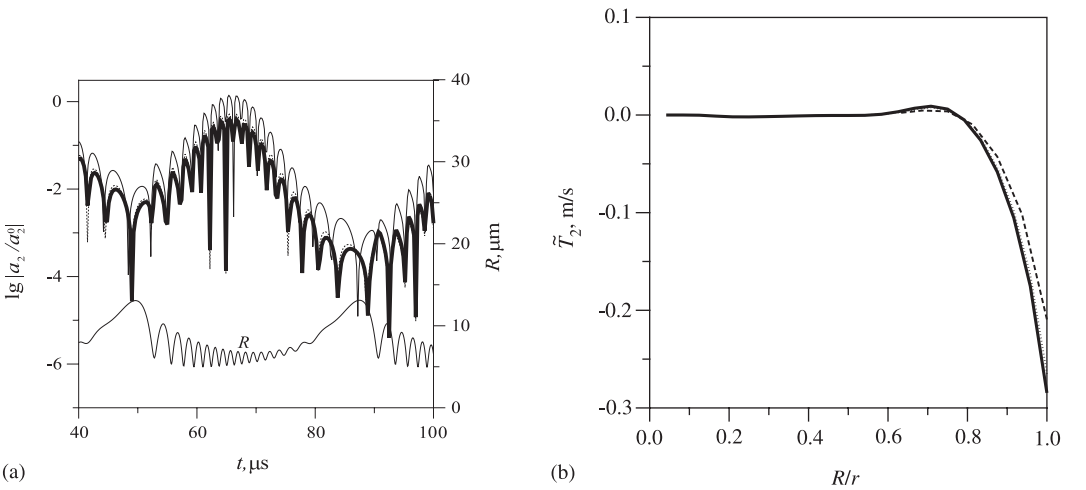

Figure 6. Same as in Figure 5 but under $t_f = 100$ μs and in (a) thin solid line corresponds to $N = 8$, in (b) dotted curve corresponds to $N = 24$.

The values of N and T for numerical solution of problem 2 in $0 \leqslant t \leqslant t_f$ with criterion (24) where $\varepsilon = 10^{-3}$ under $t_f = 40$ and 100 μs, $\Delta p/p_0 = 0.5$, 1 and 3 are given in Table V. This table shows that in all the cases considered the FDM technique requires the greatest value of N to attain numerical convergence. Despite this fact its time consumption T is everywhere the

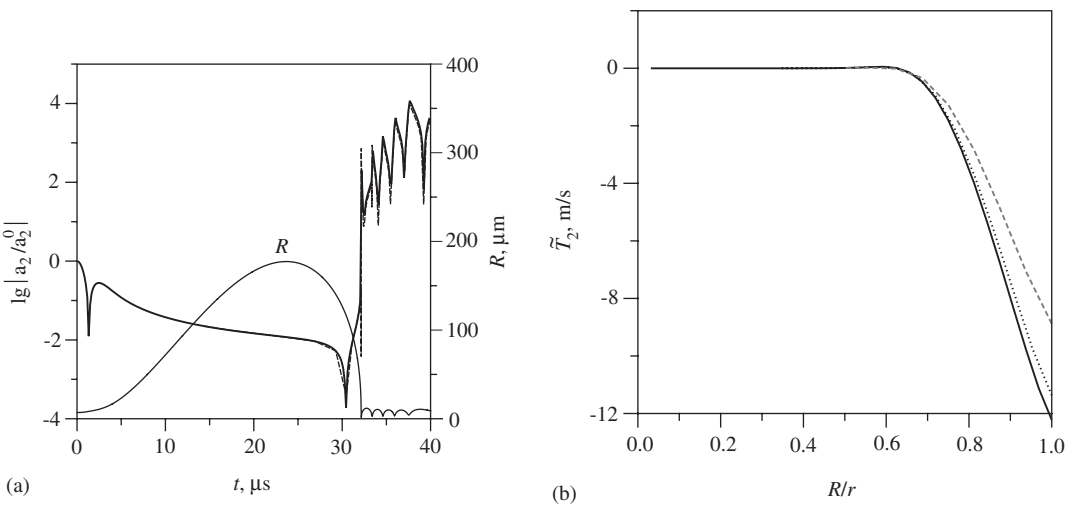

Figure 7. Time-dependences of the relative bubble shape distortion amplitude logarithm $\lg|a_2/a_2^0|$ and the bubble radius R in $0 \leqslant t \leqslant t_f$, (a) $N = 32$—dotted curve, 64—solid curve) and spatial distributions of the liquid vorticity function $\tilde{T}_2(\xi, \tau)$ at the instant t_f, (b) $N = 32$—dashed curve, 64—dotted curve, 128—solid curve) by the FDM technique under $\Delta p = 3$ bar, $t_f = 40$ μs.

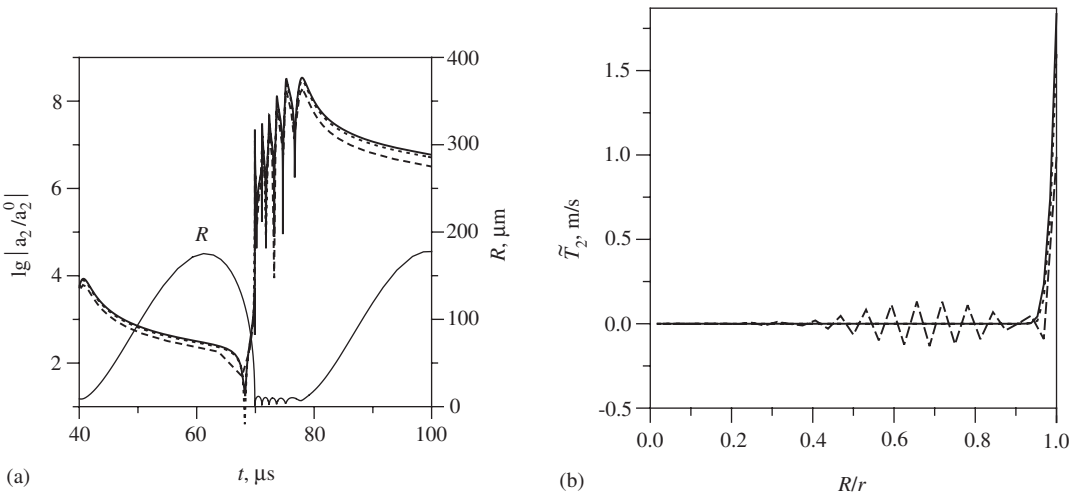

Figure 8. Same as in Figure 7 but under $t_f = 100$ μs and in (a) dashed curve corresponds to $N = 32$, dotted curve to 64, solid curve to 128.

least. The case of $\Delta p/p_0 = 3$ is most difficult for computation due to developing instability. In this case all the techniques except the FDM one fail to give numerical solution for $t_f = 100$ μs within reasonable computational time consumption. Moreover, the GM technique fails even

Table III. Computational time consumption T of a technique to solve problem 2 in $0 \leqslant t \leqslant t_f = 40\,\mu s$ under some N and $\Delta p/p_0$.

N	$\frac{\Delta p}{p_0}$	Technique			
		FDM	GM	CMd	CM
8	0.5	<1	17	13	24
	1	1	35	26	40
	3	<1	47	12	15
16	0.5	<1	43	100	120
	1	1	96	250	300
	3	1	76	90	100
24	0.5	<1	90	450	480
	1	2	210	980	970
	3	1	130	520	600
32	0.5	1	170	1600	1660
	1	2	460	2660	2780
	3	2	210	1900	2260
48	0.5	3	420	13 800	14 800
	1	6	1200	15 900	16 600
	3	3	500	11 500	13 200
64	0.5	6			
	1	11			
	3	4			
128	0.5	33			
	1	53			
	3	20			
256	0.5	200			
	1	290			
	3	100			

when $t_f = 40\,\mu s$. In the case of stable oscillations the most efficient FDM technique is followed by GM one. Two techniques based on the CM have no any significant advantage over each other.

Thus, the results presented above allow one to conclude that while solving the problem of dynamics of a bubble under harmonic liquid pressure variation in the interval $0.5 \leqslant \Delta p/p_0 \leqslant 3$ the FDM technique is again most efficient in every respect.

It should be noted that, according to Tables II and V, the dependence of the values of N and T required by a technique to solve problems 1, 2 in the interval $0 \leqslant t \leqslant t_f$ with criterion (24) on the length of this interval is stronger for the CM and CMd techniques than is for the FDM and GM ones. It follows that the FDM and GM techniques are more preferable for applying in large temporal intervals.

Table IV. Same as in Table III but for $t_f = 100\ \mu s$.

N	$\frac{\Delta p}{p_0}$	Technique			
		FDM	GM	CMd	CM
8	0.5	<1	38	24	18
	1	1	92	60	50
	3	1	96	25	21
16	0.5	1	77	180	160
	1	2	220	480	450
	3	2	160	200	180
24	0.5	1	160	1000	950
	1	3	470	1900	1800
	3	3	260	1300	1200
32	0.5	2	280	4900	4100
	1	5	820	5400	6000
	3	3	430	8600	9500
48	0.5	6	690	37 100	37 000
	1	14	2100	36 600	39 000
	3	7	1060	$>2.9 \times 10^5$	$>1.8 \times 10^5$
64	0.5	11			
	1	25			
	3	10			
128	0.5	67			
	1	125			
	3	40			
256	0.5	470			
	1	680			
	3	200			

Table V. N and time consumption T required by a technique to solve problem 2 in $0 \leqslant t \leqslant t_f$ with criterion (24) where $\varepsilon = 10^{-3}$ under some t_f and $\Delta p/p_0$.

t_f (μs)	$\frac{\Delta p}{p_0}$	Technique							
		FDM		GM		CMd		CM	
		N	T	N	T	N	T	N	T
40	0.5	64	5	16	40	32	1570	16	120
	1	128	53	24	210	16	250	16	300
	3	512	550	>48	$>10^4$	32	1900	32	2300
100	0.5	64	10	24	160	>48	$>3.6 \times 10^4$	24	940
	1	128	130	24	470	24	1900	24	1800
	3	512	1130	>48	$>10^5$	>48	$>2.9 \times 10^5$	>48	$>1.8 \times 10^5$

4. CONCLUSION

Comparison of efficiency of several numerical techniques for the liquid vorticity computation within approximation of Prosperetti [4] has been performed. The techniques based on the finite-difference [15], Galerkin and collocation methods have been considered. Two variants of using the collocation method, with [16] and without differentiation of the integral boundary condition, have been studied. Sinus-functions have been taken as the basis in the technique utilizing the Galerkin method. Solutions of two problems, decay of a small distortion of the spherical surface of a bubble and dynamics of a bubble under harmonic liquid pressure variation in the regime of SBSL [1, 2], for a number of values of their parameters have been used to compare efficiency of the techniques. In all the cases, the technique [15] based on the finite-difference method has been found to be much more (five and even more times) preferable in view of the computational time consumption. In applications this advantage will be still more significant due to the fact that the finite-difference expressions are definitely simpler to obtain and to code. It should be emphasized that this result is in some sense opposite to that stated in Reference [17] for the numerical techniques of the heat conduction computation in bubble dynamics because equations of heat conduction and vorticity are to some extent similar to one another. According to Kamath and Prosperetti [17], in the case of heat conduction the finite-difference technique is the least efficient.

The relation between efficiency of other techniques is not so clear. It can just be noted that while using the Galerkin method the number of the basis functions necessary to attain the solution of a prescribed accuracy appears to be less dependent on the length of the temporal interval.

ACKNOWLEDGEMENTS

This work was supported in part by the Russian Foundation of Basic Research (project 02-01-00100), the Program of Basic Research of the RAS (project 'Dynamics of non-spherical gas and vapour bubbles in a liquid under strong and super-strong enlargement-compression').

REFERENCES

1. Putterman SJ, Weninger KP. Sonoluminescence: how bubbles turn sound into light. *Annual Review of Fluid Mechanics* 2000; **32**:445–476.
2. Margulis MA. Sonoluminescence. *Physics-Uspekhi* 2000; **43**(3):259–282.
3. Taleyarkhan RP, West CD, Cho JS, Lahey Jr RT, Nigmatulin RI, Block RC. Evidence for nuclear emissions during acoustic cavitation. *Science* 2002; **295**:1868–1873.
4. Prosperetti A. Viscous effects on perturbed spherical flows. *Quarterly Applied Mathematics* 1977; **34**:339–352.
5. Lamb H. *Hydrodynamics* (6th edn). Dover: New York, 1945.
6. Benjamin TB. Note on shape oscillations of bubbles. *Journal of Fluid Mechanics* 1989; **203**: 419–424.
7. Longuet-Higgins MS. Monopole emission of sound by asymmetric bubble oscillations. Part 1. Normal modes. *Journal of Fluid Mechanics* 1989; **201**:525–541.
8. Kang IS, Leal LG. Bubble dynamics in time-periodic straining flows. *Journal of Fluid Mechanics* 1990; **218**: 41–69.
9. Mei CC, Zhou X. Parametric resonance of a spherical bubble. *Journal of Fluid Mechanics* 1991; **229**:29–50.
10. Brenner MP, Lohse D, Dupont T. Bubble shape oscillations and the onset of sonoluminescence. *Physical Review Letters* 1995; **75**(5):954–957.
11. Hilgenfeldt S, Lohse D, Brenner M. Phase diagrams for sonoluminescing bubbles. *Physics of Fluids* 1996; **8**:2808–2826.
12. Roberts PH, Wu CC. The decay of bubble oscillations. *Physics of Fluids* 1998; **10**:3227–3229.

13. Wu CC, Roberts PH. Bubble shape instability and sonoluminescence. *Physics Letters A* 1998; **250**:131–136.
14. Prosperetti A, Crum LA, Commander KW. Nonlinear bubble dynamics. *Journal of the Acoustical Society of America* 1988; **83**(2):502–514.
15. Aganin AA, Malachov VG, Toporkov DJ. A technique of solving problems of dynamics of a gas bubble in a viscous liquid under small distortions of its spherical shape. In *Dynamika gazovich puzirkov i aerozoley*. Kazanskiy gosudarstvenniy universitet im. V.I. Ulyanova-Lenina: Kazan, 2003; 23–41.
16. Hao Y, Prosperetti A. The effect of viscosity on the spherical stability of oscillating gas bubbles. *Physics of Fluids* 1999; **11**(6):1309–1317.
17. Kamath V, Prosperetti A. Numerical integration methods in gas bubble dynamics. *Journal of the Acoustical Society of America* 1989; **85**(4):1538–1547.
18. Hairer E, Nörsett SP, Wanner G. Solving ordinary differential equations I. *Nonstiff Problems*. Springer: Berlin, Heidelberg, 1987; 512.

